Engineering Structural Dynamics of Zirconium Metal-Organic Frameworks Based on Natural C4-linkers

Sujing Wang, Nertil Xhaferaj, Mohammad Wahiduzzaman, Kolade Oyekan, Xiao Li, Kevin Wei, Bin Zheng, Antoine Tissot, Jérôme Marrot, William Shepard, et al.

Engineering Structural Dynamics of Zirconium Metal-Organic Frameworks Based on Natural C4-linkers

Sujing Wang[1,2], Nertil Xhaferaj[1], Mohammad Wahiduzzaman[3], Kolade Oyekan[4], Xiao Li[5], Kevin Wei[4], Bin Zheng[3], Antoine Tissot[1], Jérôme Marrot[6], William Shepard[7], Charlotte Martineau-Corcos[6,8], Yaroslav Filinchuk[5], Kui Tan[4]*, Guillaume Maurin[3]*, Christian Serre[1]*

[1]Institut des Matériaux Poreux de Paris, UMR 8004 CNRS, Ecole Normale Supérieure, Ecole Supérieure de Physique et de Chimie Industrielles de Paris, PSL Université, 75005 Paris, France.

[2]Hefei National Laboratory for Physical Sciences at the Microscale, University of Science and Technology of China, Hefei, China

[3]Institut Charles Gerhardt, Montpellier UMR 5253 CNRS ENSCM UM, Université Montpellier, Place Eugène Bataillon, 34095 Montpellier cedex 05, France.

[4]Department of Materials Science & Engineering, University of Texas at Dallas, Richardson, Texas 75080, USA.

[5]Institute of Condensed Matter and Nanosciences, Université catholique de Louvain, place L. Pasteur 1, B-1348 Louvain-la-Neuve, Belgium

[6]Institut Lavoisier de Versailles, UMR 8180 CNRS, Université de Versailles Saint-Quentin-en-Yvelines, Université Paris-Saclay, 78035 Versailles, France.

[7]Synchrotron SOLEIL-UR1, L'Orme des Merisiers, Saint-Aubin, BP 48, 91192, Gif-Sur-Yvette, France.

[8]CEMHTI, UPR 3079 CNRS, 45071 Orléans CEDEX 2, France.

*E-mail: kuitan@utdallas.edu, guillaume.maurin1@umontpellier.fr, christian.serre@ens.fr

ABSTRACT

Engineering the structural flexibility of MOF materials for separation-related applications remains a great challenge. We present here a strategy of mixing rigid and soft linkers in a MOF structure to achieve tunable structural flexibility, as exemplified in a series of stable isostructural Zr-MOFs built with natural C4 linkers (fumaric acid, succinic acid and malic acid). As shown by the differences in linker bond stretching and rotational freedom, these MOFs display distinct responsive dynamics to external stimuli, namely temperature or guest adsorption. Comprehensive *in-situ* characterizations reveal a clear correlation between linker character and MOF dynamic behavior, which leads to the discovery of a multivariate flexible MOF. It shows an optimal combination of both good CO_2 working capacity and significantly enhanced CO_2/N_2 selectivity . In principle, it provides a new avenue for potentially improving the ability of microporous MOFs to separate other gaseous and liquid mixtures.

INTRODUCTION

Flexible metal-organic frameworks (MOFs) or porous coordination polymers (PCPs) represent a particular subgroup within the class of the hybrid materials, namely the third generation compounds or soft porous crystals (SPCs).[1-2] In contrast to the first and second generations,[3-5] these materials display intriguing structural dynamics in response to external stimuli, such as guest molecule variations,[6-11] light,[12-13] temperature,[14-16] electrical field[17] and pressure.[18-21] Consequently, numerous unique and unprecedented attributes have been discovered with regard to their applications in areas such as separation, sensors, catalysis, and biomedicine.[22-25] In this context, controlled inducement of the structural flexibility during MOF synthesis was regarded as an attractive strategy for targeting a given application. However, successful implementation remains a great challenge.

There are four major categories of flexibility identified for MOFs in the literature, including breathing, swelling, linker rotation and sub-network displacement.[26-28] In the case of breathing MOFs, such as the MIL-53 (Materiaux from Institute Lavoisier) series, the influence of phenylene ring rotation about its C-C axis to different extends are responsible for the notable changes in the unit cell.[14] A recent discovery of a breathing MOF displaying negative gas adsorption properties, namely DUT-49 (Dresden University of Technology No. 49),[29] showed that metal node rotation could also lead to structural breathing, with a noticeable induced-bending of the biphenyl moiety in the linker . For the swelling examples, such as MIL-88, metal node rotation is the sole driving force, with a very limited contribution of the linker to the overall change in the unit cell parameters .[30] Finally, linker rotation that does not induce significant changes in the unit cell has been observed in some non-breathing/swelling MOF structures such as ZIF-8 and MIL-140s, which are built with linkers containing rigid aromatic centers.[28]

To the best of our knowledge, each flexible MOF reported has its individual combination of linker selection and inorganic building block. Consequently, the

corresponding structural flexibility can only be tuned by the introduction of attached functional groups. The resulting linker bond distortion and bending are thus unrelated to the local freedom of bond stretching and rotation. On the other hand, flexible aliphatic linkers with linear or cyclic alkane centers that possess greater bond stretching and rotational freedom were expected to favor the generation of dynamic structures. However, relevant studies in this field remain scarce.[23, 31-33]. Hence, it is very difficult to investigate the impact of linkers' freedom of bond stretching and rotation on the softness of a given MOF type when the rigid and flexible linker pair is unable to generate isostructural MOFs. In this regard, it would be of great interest to engineer the structural flexibility in a series of isostructural MOFs using the same inorganic building block, and linkers of similar molecular size and configuration but with different degrees of structural freedom (in both bond stretching and rotation), in order to understand how the local and structural dynamics of the architectures are governed by the linker characters.

To achieve this goal, the expected MOF candidates should fulfill the following requirements: 1) isostructural analogues built with linkers of different degrees of freedom; 2) an inorganic building block exhibiting a possible plane of symmetry, allowing the cooperative movements of various bonds involved; 3) frameworks featuring an accessible porosity to certain stimuli that can easily be detected, analyzed and compared; 4) compounds being robust to avoid any structural deterioration.

Herein, we present a series of isostructural MOFs based on 10-connected Zr_6 clusters and natural C4 carboxylate linkers with linear aliphatic chains, denoted as MIP-203-F, MIP-203-S, and MIP-203-M (MIP stands for the Materials of the Institute of Porous Materials from Paris, F for fumaric acid, S for succinic acid, and M for malic acid), designed to engineer structural flexibility based on the nature and degree of freedom of the linker. While MIP-203-F is constructed using double-bonded fumarate and MIP-203-S is built with single-bonded succinate, MIP-203-M contains a sparse framework displaying multivariate flexibility[28], with 2/3 fumarate and 1/3 malate as linkers resulting from a particular *in situ* dehydration reaction of malic acid into

fumaric acid. The response of these MOFs' structural dynamics to external stimuli, namely temperature and guest adsorption, has been characterized in detail in order to investigate the possible correlation between linker degree of freedom and MOF dynamics. MIP-203-F shows noticeably more swelling flexibility compared to MIP-203-S due to the differences between rigid fumarate and flexible succinate. The effective combination of two types of flexibility in MIP-203-M, namely swelling and bond distortion/bending, results finally in the best CO_2/N_2 selectivity. This suggests a new avenue for improving the ability of microporous MOFs to facilitate the separation of a wide range of gaseous or vapors mixtures. Moreover, these Zr-MOFs feature good chemical stability, cheap and biocompatible natural linkers, and green, scalable synthetic routines, all of which make them promising candidates for future practical applications.

RESULTS AND DISCUSSION

Among the reported inorganic building blocks having a possible symmetry plane, the Zr_6 cluster is one of the best options owing to its high connectivity and chemical stability, natural abundance, and low toxicity. The $Zr_6O_4(OH)_4$ cluster is one of the most common secondary building units (SBUs) reported in the literature.[34-35] The varying node connectivity, including the 12-, 10-, 8-, 6-, and 4-connected Zr_6-oxocluster in MOFs, allow a high degree of tunability of the corresponding MOFs structures, which provides a better opportunity to achieve a flexible crystal architecture. The 12-connected Zr_6 cluster has the densest connection environment and thus less freedom and space for configuration rearrangement. Alternatively, reducing the connectivity of the Zr_6 cluster could be more favorable to introduce structural flexibility.[11] In view of these factors, Zr-MOFs with low connectivity SBUs were preferentially considered as the model compounds.

Judicious use of flexible linkers has already been demonstrated to be an efficient strategy for generating soft MOFs structures when the inorganic SBUs are rigid.[23, 28]

Among the reported flexible linkers, naturally occurring compounds are of particular

interest since they are bio-compatible and thus efficiently reduce the toxicity of the resulting MOFs. In the limited cases of existing Zr-MOFs composed of natural acids,[34] fumaric acid and its derivatives are dominant despite the fact that they all share the 12-fold connectivity, which highlights the controllable crystallization of Zr-fumarate type frameworks,[36-39] as well the rigid structural character of fumaric acid, which is the same as evidenced in other MOFs.[24-25, 40] On the contrary, succinic acid, which behaves as a soft molecular spring as seen in Co-MOFs,[41-42] has molecular lengths and configurations similar to those of fumaric acid. The most noticeable difference between succinic acid and the double-bonded fumaric acid is the former's single-bonded carbon skeleton, which usually exhibits greater freedom of stretching and rotation. In view of these features, fumaric and succinic acids, as the simplest pair of rigid and flexible natural carboxylic linkers respectively, were selected for their typicality and suitability for the aforementioned target. Additionally, malic acid, a succinic acid derivative with a hydroxyl group on the alkane chain, was also used to check the impact of the side functional group on the flexibility of the architecture.

Fumaric acid (Fig. 1a) was first used to react with $ZrCl_4$ as model reaction. Formic acid has been proven to be a modulating agent to generate the 12-connected structure with improved crystallinity in the preparation of Zr-Fumarate (as known as MOF-801).[43] We expected that the increase in the amount of formic acid in the reaction solution could decrease the connectivity of the Zr_6 cluster, leading to less rigid structures with lower structural symmetry. Pure formic acid was used as solvent in this case since it has been shown to be an efficient modulator for preparing group IV metal-based MOFs.[38, 44] As expected, instead of forming the well-known Zr-Fumarate structure, MIP-203-F, a new phase with lower structural symmetry was obtained (Fig.1b). When succinic acid was used under the same reaction conditions, a clear solution was observed without any solid product, possibly due to the much greater solubility of succinic acid in formic acid. After optimizing the reactant concentrations and the ratio between $ZrCl_4$ and succinic acid, the expected isostructural product was successfully obtained. The synthesis of MIP-203-M could

be achieved by tuning the reactant ratio under similar conditions (see SI for detail).

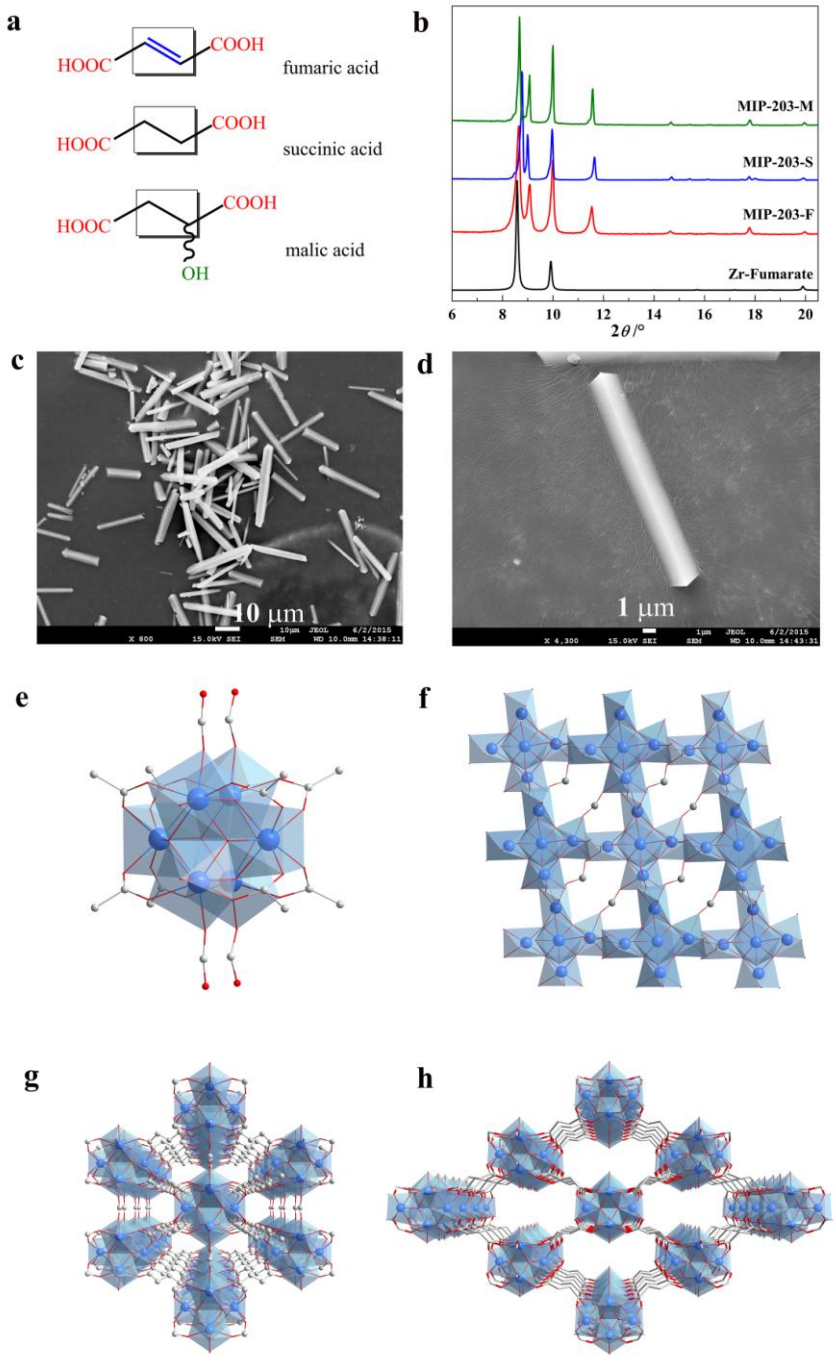

Figure 1. Structure details of MIP-203. (a) Chemical structures of the three naturally occurring dicarboxylic acids used in this work. (b) PXRD pattern comparison ($\lambda_{Cu} \approx 1.5406$ Å) between Zr-Fumarate and MIP-203s. (c) and (d) Scanning electron microscopy (SEM) images of MIP-203-F with different magnifications. (e) The 10-connected $Zr_6(\mu_3\text{-}O)_4(\mu_3\text{-}OH)_4$ SBU showing eight linker carboxylates and two pairs of bridging formates in MIP-203-F. (f) and (g) Framework viewed along the *a*-axis and *b*-axis respectively, clearly showing the bridging formates in

MIP-203-F. (h) Framework viewed along the c-axis in MIP-203-F. Color scheme: Zr in blue, O in red and C in gray (hydrogen atoms are omitted for clarity).

The crystal structure model of MIP-203 was initially determined on MIP-203-S using a dual computational and experimental approach developed on the principle of Automated Assembly of Structure Building Unit (AASBU) theory that combines high-resolution powder X-ray diffraction data and our *in-house* crystal structure prediction software.[45] Afterwards, needle-like single crystals of MIP-203-F with a homogeneous size and shape distribution (Fig. 1c and 1d) were subjected to the synchrotron diffraction single crystal data collection with a micro-focused X-rays on the Proxima 2A beamline (Synchrotron SOLEIL, France),[46] in order to experimentally confirm the major framework connectivity of the simulated structural model.

Since the three MIP-203 compounds are isostructural, MIP-203-F was used as an example to detail their structural features. It was found that MIP-203-F, $Zr_6(\mu_3\text{-}O)_4(\mu_3\text{-}OH)_4(\text{fumarate})_4(\text{formate})_2(OH)_2(H_2O)_2$, crystallizes in an orthorhombic *Immm* space group with unit cell parameters of a = 10.000(2) Å, b = 11.940(2) Å, c = 19.829(11) Å and V = 2367.6(15) Å^3. The Zr_6 SBUs (Fig. 1e) were interconnected with one another by both fumarate and formate linkers, resulting in the final three-dimensional (3D) framework. It is, to the best of our knowledge, the first time that a Zr_6 SBU with mixed linkage from two highly dissimilar linkers in term of shape, configuration and connectivity was generated using direct synthesis for Zr-MOFs. Formate serves as the auxiliary ligand connecting the adjacent SBUs along the *c*-axis. However, their presence blocks the window of the pores along the *a*-axis (Fig. 1f). When the structure is viewed along the *b*-axis (Fig. 1g), formates are shown to occupy the middle of the large rhombic channels, dividing them into two 4 Å sized triangular channels, which is also observed in the case of UiO-66(Zr) type structures.[47] Due to the presence of the terminal OH^-/H_2O pairs in the SBU, there exist rhombic channels running along the *c*-axis without any blocking species (Fig. 1h). Simulation results indicate that both MIP-203-F and MIP-203-S possess almost identical pore volumes (0.27 and 0.25 cm^3 g^{-1} for –F and –S, respectively) and pore

sizes estimated from the PSD plots (largest pore diameters ~5 Å, Figure S3). However, due to the difference between C-C single and C=C double bonds, fumaric and succinic acids show slightly different conformations (see Figure S4-S6), resulting in the pore shape and dimension of the corresponding MOFs to vary to some extent (Figure S3).

An *in situ* dehydration reaction occurred when malic acid was introduced in the synthesis of MIP-203-M, leading to the transformation of 2/3 malic acid into fumaric acid. MIP-203-M can therefore be considered as the corresponding product of replacing 1/3 fumarate in MIP-203-F by malate, as evidenced by solid-state NMR data (Figure S7). The coexistence of fumarate and malate in MIP-203-M makes it an unusual example of the MOF framework that shows multivariate flexibility through direct synthesis.

Thermal and chemical stability tests of MIP-203s were carried out before investigating and comparing the response to different external stimuli of the MIP-203s. The influence of thermal activation of the as-synthesized samples was first studied. As shown in Fig 2a, the as-synthesized MIP-203-F sample displays four PXRD peaks at low angle, i.e. 8.46, 8.94, 9.86 and 11.36° corresponding to the (011), (002), (101) and (110) Bragg peaks, respectively. After activating the sample at 100 °C under vacuum, the distinct shifts to higher angle domains for the peaks at 8.73 and 11.56° were observed., which could be ascribed to the notable decrease of the *b* unit-cell parameter in the activated sample (11.856 Å) in comparison with that of the as-synthesized one (12.246 Å). The larger change in *b* compared to *a* and *c* could be explained by the weaker connection along *b*-axis in the crystal structure while the presence of bridging formates undoubtedly enhances the overall rigidity of the *a*-*c* plane. Similar observation was noticed between the as-synthesized and activated samples of both MIP-203-S and MIP-203-M (Fig 2b and 2c).

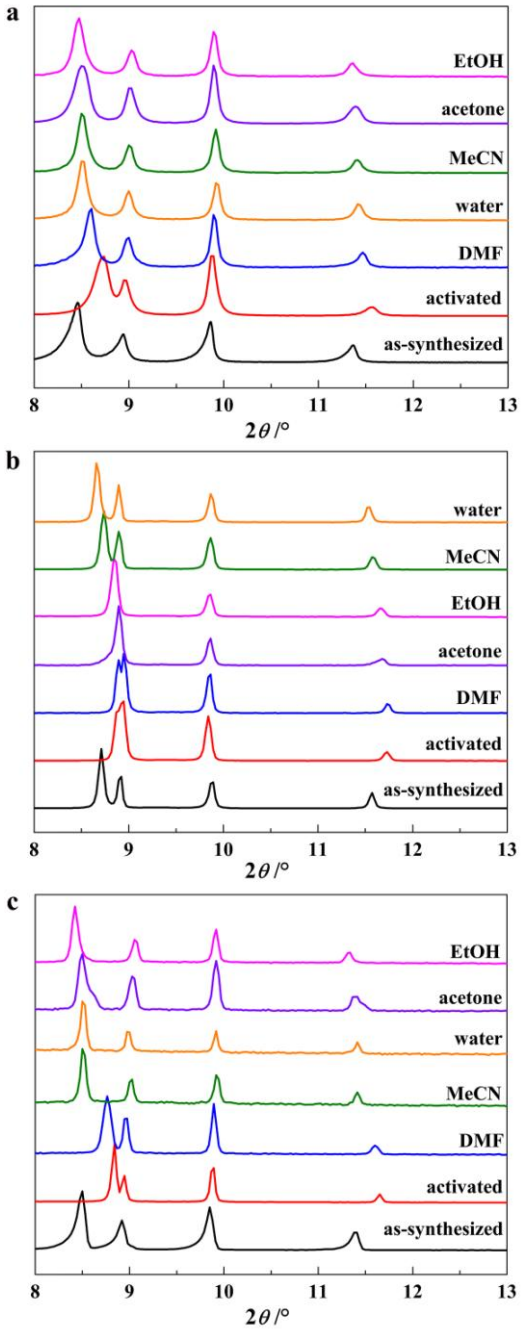

Figure 2. Structural response at room temperature of MIP-203s to liquid external stimuli (PXRD, $\lambda_{Cu} \approx$ 1,5406 Å). **a**. MIP-203-F in different solvents. **b**. MIP-203-S in different solvents. **c**. MIP-203-M in different solvents.

The cell volume of the activated samples decreased by 57.6 $Å^3$/2.4%, 73.9 $Å^3$/3.1% and 80.4 $Å^3$/3.4% for MIP-203-F, -M and -S, respectively, in comparison with those of the as-synthesized ones, suggesting their similar structural contraction abilities upon thermal stimulus (Table S2, S3 and S4).

In situ Raman spectroscopy was further employed to monitor the changes occurring in specific bonds in the MOF structure upon activation. Figs 3a and 3b present the most pronounced changes in the range of 1800-1200 cm^{-1} caused by *in situ* activation of the sample at 100 °C (see full spectra in Supporting information). In comparison to the as-synthesized MIP-203-S, the peak centers of the carboxylate stretching bands ν_{as}(COO) and ν_{s}(COO) in the activated sample are blue-shifted of 7 cm^{-1} and 6 cm^{-1}, respectively, indicative of the bond hardening due to structural contraction upon removal of the solvents. The corresponding ν_{s}(COO) change in MIP-203-F sample is only 3 cm^{-1} and ν_{as}(COO) peak intensity is too weak to be addressed, which evidences a much less pronounced bond change compared to that of MIP-203-S. Furthermore, a band at 1289 cm^{-1} for activated MIP-203-S with a 11 cm^{-1} red-shift compared to the as-synthesized one was assigned to the vibration mode that involves -CH_2 wagging coupled with C-C-C-C stretching (see the attached videos 1 and 2). On the contrary, only 7 cm^{-1} difference (1277 to 1284 cm^{-1}) for the -CH wagging in C-C=C-C was detected for MIP-203-F before and after the thermal activation. This mode has been shown to be very sensitive to changes in the bond angle of the carbon chain.[48] As shown in Figures 3a and 3b by DFT calculation, when the angles p and q (p and q are bond angles of the C4 skeleton of the linker) are decreased by ~2° and ~4° respectively for fumaric acid, and ~5° and ~5° for succinic acid, its frequency shifts downward by ~10 cm^{-1} and ~15 cm^{-1} in fumaric acid and succinic acid, respectively. The trend of these shifts is in good agreement with the experimentally observed values. It also matches well the similar observation reported on other flexible MOFs.[48] The above results point out the origin of different structural contraction response arising from the distortion of the C-C=C-C and C-C-C-C chains for MIP-203-F and MIP-203-S, respectively. It indicates that the local stretching and vibration freedoms of the succinate single-bonded skeleton are more pronounced than those of the fumarate double-bonded one. This observation is also supported by a much smoother evolution of the DFT-calculated potential energy for the succinate-cluster model vs the fumarate-one when one varies the dihedral angle of the organic linker from its minimum-energy value, suggesting a higher ability of distortion for the succinate

linker (Figure S4-S6). The spectra of MIP-203-M are dominated by a strong fluorescence signal and thus are not presented here.

The structural responses of MIP-203s to exposure to liquid guest molecules were then investigated. Activated samples of these three MOFs were exposed to diverse solvents and high-resolution PXRD patterns were collected with wet samples sealed in capillaries. The corresponding results are shown in Fig. 2 and the indexing summary was listed in Table S2-S4.

When the dried MIP-203-F sample was exposed to diverse solvents, the MOF framework allowed all the solvent molecules entering the pore. The molecular size and shape of the solvent did not show notable effect on the structural variation of the MOF. A continuous increase of their unit cells along the *b* axis was observed following the order of N,N-dimethylformamide (DMF) < water < acetonitrile < acetone < ethanol (Table S2). It is an indicative evidence that the MIP-203-F presents a tunable structural swelling property.

In contrast, dried MIP-203-S sample displayed strict compatibility to solvent molecules according to their sizes and shapes (Fig. 2b). Solvent molecules with larger sizes or branched shapes, such as DMF, acetone and ethanol, could hardly enter the dynamic pore of MIP-203-S, evidenced by the comparatively minimal changes in its PXRD pattern. It is possibly that the single-bonded aliphatic linkers tend to stay in a closely packed configuration when the pores are in a guest-free from. For the loading of accessible solvent molecules, the MOF structure expands dramatically along with a notable increase of the *b* unit cell parameter. Correspondingly, their PXRD pattern show marked changes compared to that of the activated sample and are similar to that of the as-synthesized one. Therefore, this selective inclusion of solvent molecules based on their sizes and shapes reflects the effect of the local bond distortion/bending generated from the succinate aliphatic chain rather than the framework structural swelling.

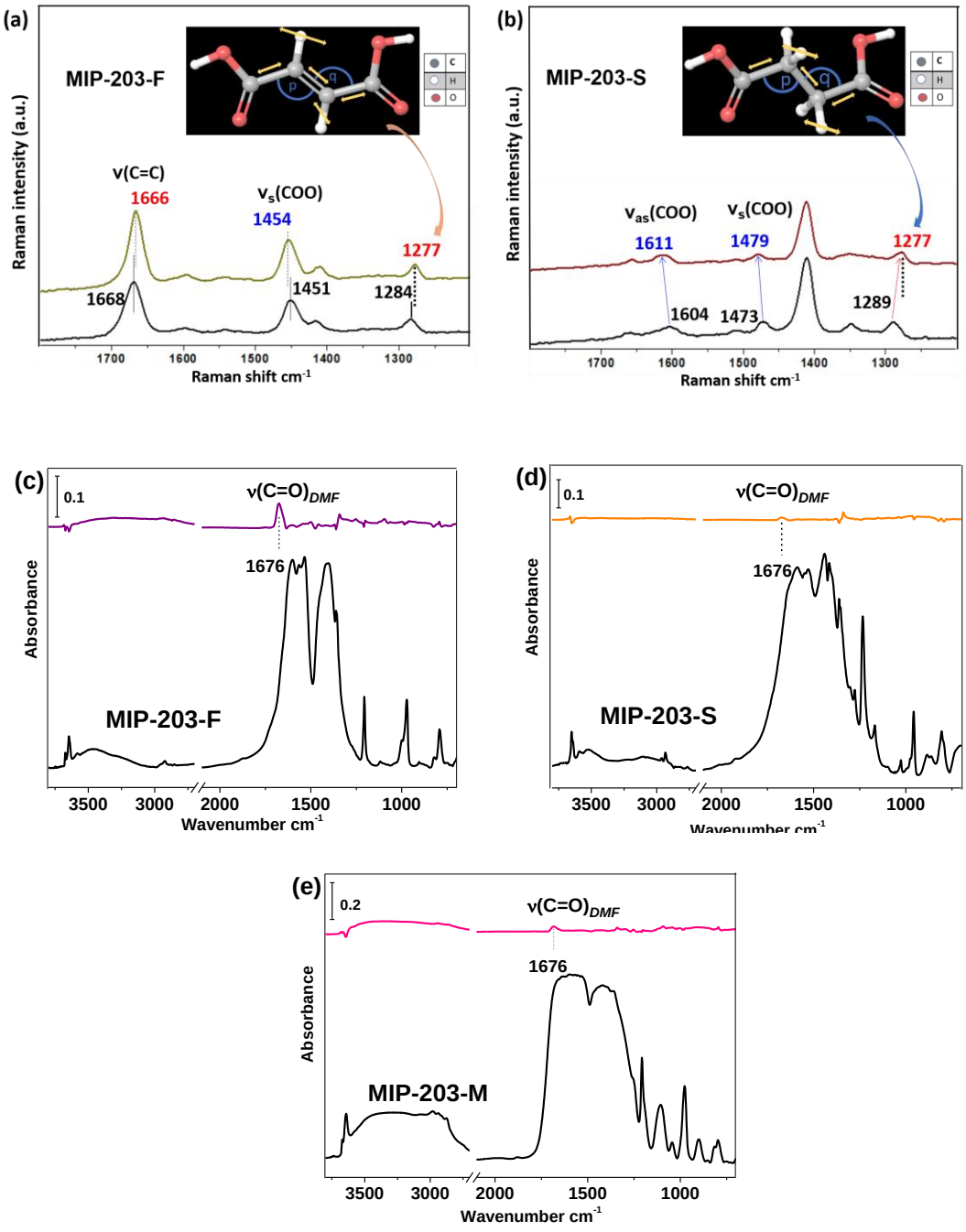

Figure 3. Raman spectra of MIP-203-F (a) and MIP-203-S (b) in as-synthesized (top lines) and dried (bottom lines) form upon *in situ* activation. The spectra are collected at room temperature. *In situ* IR spectra of adsorbed DMF in MIP-203-F (c), MIP-203-S (d) and MIP-203-M (e), referenced to the activated MOFs (bottom black lines) under vacuum.

In the case of MIP-203-M, the response to the loading of solvent molecules exhibits a combined effect observed in MIP-203-F and MIP-203-S. As shown in Fig. 2c, solvent molecules with large sizes and branches, such as DMF, have a lesser effect on the

MOF structure expansion, mainly due to the local bond distortion/bending and steric hindrance of the malate linker. Smaller solvent molecules could diffuse more easily into the MOF pore. In other words, a good structural swelling flexibility of the framework associated with an appropriate local bond distortion/bending towards guest molecules has been achieved in MIP-203-M.

In situ infrared (IR) spectroscopy was employed to probe the interactions between the guest solvent molecules and the framework. DMF was chosen as the representative solvent to study its adsorption in the selected MOFs, due to the structural responses of these MOFs to DMF solvent showing significant variation (Fig.2). A vapor pressure of 4 Torr of DMF was introduced into the activated MOFs samples for ~5 min to reach the adsorption equilibrium with the adsorbed DMF was characterized by a carbonyl stretching band ν(C=O) at 1676 cm^{-1}, shifted by 39 cm^{-1} from the center of the gas phase band (Fig. 3 and Figure S8). A comparison of the intensities of the ν(C=O) band at 1676 cm^{-1} in IR spectra of Fig. 3 indicates that the uptakes of adsorbed DMF in these three samples exhibits the following trend: MIP-203-F > MIP-203-M > MIP-203-S.

It is well-documented in the literature that flexible MOFs show a great promise in dynamic separation of practical gases mixtures,[35, 49-51] such as carbon dioxide over nitrogen in the post-combustion process. Considering the distinct response of MIP-203s to thermal activation and the adsorption of liquid guest molecules shown above, we speculated that similar behaviors could be observed when exposed to gas phase guest molecules. Single component gases sorption measurements of N_2 and CO_2 under various conditions were performed. Nitrogen adsorption data collected at 77 K show clearly that the pores in MIP-203-F are accessible to N_2 molecules, displaying a typical type I adsorption isotherm associated with a Brunauer-Emmett-Teller (BET) area of 430 m^2 g^{-1} and a total pore volume of 0.24 cm^3 g^{-1}. In a sharp contrast, MIP-203-S did not show any accessible porosity to N_2 at 77 K (Fig. 4a). It is likely that soft single-bonded C4 skeleton of succinic acid that can distort more than fumaric acid with C=C double bond. After thermal activation under

vacuum to remove the guest molecules, MIP-203-S tends to stay in a closely packed form so that it is not accessible to nitrogen. When the adsorption temperature was increased to 273 K, the thermodynamic motions of single-bonded aliphatic chain of succinate resulted in a slight increase of N_2 uptake (Figure S12). The much higher uptake for MIP-203-F at 273 K suggests its more pronounced swelling ability towards nitrogen sorption stimuli or larger pore opening in its activated form. In the case of MIP-203-M, it shows a BET area of 380 m^2 g^{-1} and pore volume of 0.21 cm^3 g^{-1} comparable to that of MIP-203-F, indicating the beneficial effect of the fumarate content. A notable reduction of N_2 uptake was however observed at 273 K in comparison with that of MIP-203-F, showing the critical role of the soft malate content.

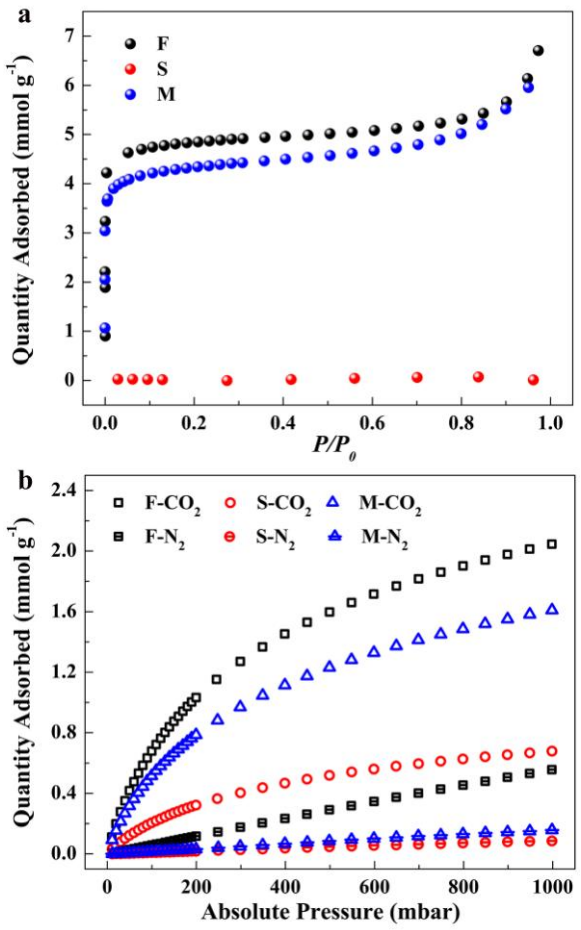

Figure 4. Single component gases adsorption behaviors of MIP-203s. **a** N_2 adsorption isotherms collected at 77 K. **b** CO_2 and N_2 adsorption isotherms collected at 298 K.

When the probe molecule was switched to the smaller-sized CO_2, the influence of linker softness on the structural dynamics is much less pronounced. MIP-203-S exhibits half the uptake of CO_2 compared to MIP-203-F over almost the entire pressure range at 273 K (Figure S13). However, a significant decrease in CO_2 uptake was observed for MIP-203-S when the adsorption temperature was increased to 298 K. The uptake at 1 bar drops by 58%, from 1.61 mmol g^{-1} at 273 K to 0.68 mmol g^{-1} at 298 K. In the case of MIP-203-F, only a 24% reduction (2.72 mmol g^{-1} to 2.05 mmol g^{-1}) in CO_2 uptake at 1 bar was observed from 273 K to 298 K. Therefore, MIP-203-F and MIP-203-S indeed display huge differences in their structural responses to gaseous guest molecules, as expected. MIP-203-M behaves more similarly to MIP-203-F than MIP-203-S, likely due to the major linker component of fumarate in its structural framework.

To check the structural response of the MOF framework in the presence of CO_2 guest molecules, *in situ* PXRD data along the adsorption of CO_2 under various pressures was collected on the three MIP-203 samples at room temperature. As shown in Figure 5, both activated MIP-203-F and MIP-203-M structures could easily swell back to the open form under a low CO_2 pressure (between 200-300 mbar), highlighting their swelling flexibility. Further increasing the CO_2 pressure did not have any notable effects on the samples' structural expansion. However, the activated MIP-203-S sample remained in its closely packed configuration throughout the entire range of CO_2 pressures applied. Even high CO_2 pressure (6 bar) was not able to reopen the framework, which is consistent with its lower CO_2 uptake compared to those of MIP-203-F and MIP-203-M under the same condition.

To evaluate the adsorption affinity, isosteric heats of adsorption (Q_{st}) were calculated with the CO_2 adsorption isotherms collected at 273 K, 298 K and 303 K in the pressure range of 0-1 bar. At zero coverage, the Qst values are 32 KJ mol^{-1}, 34 KJ mol^{-1} and 33 KJ mol^{-1} for MIP-203-F, MIP-203-S and MIP-203-M, respectively. The working capacities of CO_2 sorption (Wc(1-0.1 bar)) for three MIP-203 samples were calculated to be 1.38, 1.04 and 1.15 mmol/g for MIP-203-F, MIP-203-S and

MIP-203-M, respectively, at 273 K. The corresponding values at 298 K are 1.35, 0.47 and 1.09 mmol/g. It is interesting to note that the working capacities for both MIP-203-F and MIP-203-M showed far less dependence on the considered temperature, while the working capacity of MIP-203-S exhibited dramatic sensitivity towards the applied temperature, decreasing by more than half when the temperature increased from 273 K to 298 K.

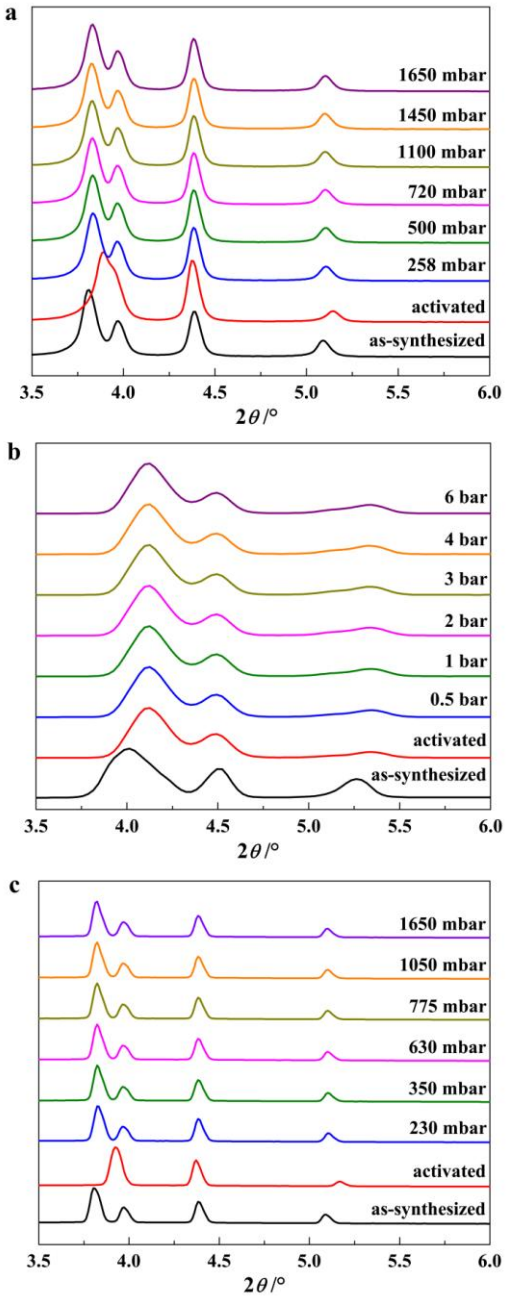

Figure 5. In situ PXRD patterns of MIP-203s along adsorption of CO_2 under different pressures at room temperature. **a** MIP-203-F. **b** MIP-203-S. **c** MIP-203-M.

Furthermore, Ideal adsorbed solution theory (IAST)[52-53] was applied to evaluate the adsorption CO_2/N_2 selectivity of MIP-203s when a binary mixture of CO_2:N_2=15:85 (v:v) at 298 K was considered (Fig. S14). The corresponding selectivities were calculated to be 15, 34 and 51 for MIP-203-F, MIP-203-S and MIP-203-M, respectively (Figure S14), which are in the usual range for MOF-based CO_2 sorbents.[54-55] It is worth noting that MIP-203-S shows a selectivity twice as high as that of MIP-203-F, highlighting the linker softness effect that interferes nitrogen from entering the pores. However, MIP-203-M outperforms MIP-203-S in terms of selectivity by a margin of 50%. The above comparison of the CO_2 working capacity and adsorption selectivity between the three MIP-203 compounds suggests that the introduction of a proper local softness into a structurally flexible MOF framework would result in a favorable combination of accessible porosity and structural dynamics, leading to an optimal balance for selective CO_2 separation in terms of working capacity and selectivity.

CONCLUSION

In summary, we report a series of flexible isostructural Zr-MOFs synthesized based on natural C4 linkers (MIP-203s), in which the structural dynamics can be engineered based on the differences in freedom of linker bond stretching and rotation between rigid fumarate and soft succinate. Comprehensive characterizations of structural responses to diverse external stimuli, including thermal changes as well as liquid and gaseous guest molecules, have been conducted to correlate the corresponding linker's flexibility with MOF dynamics. Directed by this established correlation, MIP-203-M, with a proper multivariate flexibility that efficiently combines swelling and linker distortion/bending, was evaluated for the adsorptive separation of CO_2/N_2. It not only exhibits a good working capacity for CO_2 adsorption under the working condition benefiting from the swelling of MIP-203-F framework, but also a significantly enhanced selectivity for CO_2/N_2 compared to those of the –F and –S forms, owing to the linker stretching and rotational flexibility generated from the soft succinate skeleton. In principle, this strategy could be applied to the separation of other

chemical mixtures, including liquid and gaseous phases. Therefore, it serves as a suitable example that engineering the structural flexibility of MOF materials could constitute a promising and versatile strategy for improving MOF separation performance, or even realizing new applications.

AUTHOR INFORMATION

Corresponding Authors

*christian.serre@ens.fr (C.S.)

*guillaume.maurin1@umontpellier.fr (G.M.)

*kuitan@utdallas.edu (K.T.)

ORCID

Sujing Wang: 0000-0003-0942-2907

Mohammad Wahiduzzaman: 0000-0003-2025-4115

Charlotte Martineau-Corcos: 0000-0003-1887-1042

Guillaume Maurin: 0000-0002-2096-0450

Christian Serre: 0000-0003-3040-2564

Notes

The authors declare no competing interest.

ACKNOWLEDGEMENT

The authors from France are grateful to the ANR Project MeaCoPA (ANR-17-CE29-0003) for financial support. The spectroscopic characterization and analysis (IR and Raman) were supported by the U.S. Department of Energy, Office of Science, Office of Basic Energy Sciences under Award Number DE-FG02-08ER46491

REFERENCES

1. Kitagawa, S.; Kondo, M., Functional micropore chemistry of crystalline metal complex-assembled compounds. *B. Chem. Soc. Jpn* **1998,** *71* (8), 1739-1753.
2. Bureekaew, S.; Shimomura, S.; Kitagawa, S., Chemistry and application of flexible porous coordination polymers*. *Sci.Technol. Adv. Mat.* **2008,** *9* (1), 70-71.
3. Liu, J.; Chen, L.; Cui, H.; Zhang, J.; Zhang, L.; Su, C. Y., Applications of metal-organic frameworks in heterogeneous supramolecular catalysis. *Chem Soc Rev* **2014,** *43* (16), 6011-61.
4. Horike, S.; Shimomura, S.; Kitagawa, S., Soft porous crystals. *Nat Chem* **2009,** *1* (9), 695-704.
5. Kitagawa, S.; Kitaura, R.; Noro, S., Functional porous coordination polymers. *Angew Chem Int Ed* **2004,** *43* (18), 2334-75.
6. Seo, J.; Matsuda, R.; Sakamoto, H.; Bonneau, C.; Kitagawa, S., A pillared-layer coordination polymer with a rotatable pillar acting as a molecular gate for guest molecules. *J Am Chem Soc* **2009,** *131* (35), 12792-800.
7. Loiseau, T.; Serre, C.; Huguenard, C.; Fink, G.; Taulelle, F.; Henry, M.; Bataille, T.; Férey, G., A Rationale for the Large Breathing of the Porous Aluminum Terephthalate (MIL-53) Upon Hydration. *Chem-Eur. J* **2004,** *10* (6), 1373-1382.
8. Mellot-Draznieks, C.; Serre, C.; Surble, S.; Audebrand, N.; Ferey, G., Very large swelling in hybrid frameworks: a combined computational and powder diffraction study. *J Am Chem Soc* **2005,** *127* (46), 16273-8.
9. Krause, S.; Bon, V.; Stoeck, U.; Senkovska, I.; Tobbens, D. M.; Wallacher, D.; Kaskel, S., A Stimuli-Responsive Zirconium Metal-Organic Framework Based on Supermolecular Design. *Angew Chem Int Ed* **2017,** *56* (36), 10676-10680.
10. Qin, J. S.; Yuan, S.; Alsalme, A.; Zhou, H. C., Flexible Zirconium MOF as the Crystalline Sponge for Coordinative Alignment of Dicarboxylates. *ACS Appl Mater Interfaces* **2017,** *9* (39), 33408-33412.
11. Zhang, Y.; Zhang, X.; Lyu, J.; Otake, K. I.; Wang, X.; Redfern, L. R.; Malliakas, C. D.; Li, Z.; Islamoglu, T.; Wang, B.; Farha, O. K., A Flexible Metal-Organic Framework with 4-Connected Zr6 Nodes. *J Am Chem Soc* **2018,** *140* (36), 11179-11183.
12. Brown, J. W.; Henderson, B. L.; Kiesz, M. D.; Whalley, A. C.; Morris, W.; Grunder, S.; Deng, H. X.; Furukawa, H.; Zink, J. I.; Stoddart, J. F.; Yaghi, O. M., Photophysical pore control in an azobenzene-containing metal-organic framework. *Chem Sci* **2013,** *4* (7), 2858-2864.
13. Modrow, A.; Zargarani, D.; Herges, R.; Stock, N., The first porous MOF with photoswitchable linker molecules. *Dalton Trans* **2011,** *40* (16), 4217-22.
14. Liu, Y.; Her, J. H.; Dailly, A.; Ramirez-Cuesta, A. J.; Neumann, D. A.; Brown, C. M., Reversible structural transition in MIL-53 with large temperature hysteresis. *J Am Chem Soc* **2008,** *130* (35),

11813-8.
15. DeVries, L. D.; Barron, P. M.; Hurley, E. P.; Hu, C.; Choe, W., "Nanoscale lattice fence" in a metal-organic framework: interplay between hinged topology and highly anisotropic thermal response. *J Am Chem Soc* **2011,** *133* (38), 14848-51.
16. Henke, S.; Schneemann, A.; Fischer, R. A., Massive Anisotropic Thermal Expansion and Thermo-Responsive Breathing in Metal-Organic Frameworks Modulated by Linker Functionalization. *Adv Funct Mater* **2013,** *23* (48), 5990-5996.
17. Ghoufi, A.; Benhamed, K.; Boukli-Hacene, L.; Maurin, G., Electrically Induced Breathing of the MIL-53(Cr) Metal-Organic Framework. *ACS Cent Sci* **2017,** *3* (5), 394-398.
18. Chapman, K. W.; Halder, G. J.; Chupas, P. J., Pressure-induced amorphization and porosity modification in a metal-organic framework. *J Am Chem Soc* **2009,** *131* (48), 17546-7.
19. Gagnon, K. J.; Beavers, C. M.; Clearfield, A., MOFs under pressure: the reversible compression of a single crystal. *J Am Chem Soc* **2013,** *135* (4), 1252-5.
20. Goodwin, A. L.; Keen, D. A.; Tucker, M. G., Large negative linear compressibility of Ag3[Co(CN)6]. *Proc Natl Acad Sci U S A* **2008,** *105* (48), 18708-13.
21. Yot, P. G.; Ma, Q.; Haines, J.; Yang, Q.; Ghoufi, A.; Devic, T.; Serre, C.; Dmitriev, V.; Férey, G.; Zhong, C.; Maurin, G., Large breathing of the MOF MIL-47(VIV) under mechanical pressure: a joint experimental–modelling exploration. *Chem. Sci.* **2012,** *3* (4), 1100-1104.
22. Schneemann, A.; Bon, V.; Schwedler, I.; Senkovska, I.; Kaskel, S.; Fischer, R. A., Flexible metal–organic frameworks. *Chem. Soc. Rev.* **2014,** *43* (16), 6062-6096.
23. Lin, Z. J.; Lu, J.; Hong, M.; Cao, R., Metal-organic frameworks based on flexible ligands (FL-MOFs): structures and applications. *Chem Soc Rev* **2014,** *43* (16), 5867-95.
24. Férey, G., Giant flexibility of crystallized organic–inorganic porous solids: facts, reasons, effects and applications. *New J. Chem.* **2016,** *40* (5), 3950-3967.
25. Férey, G., Structural flexibility in crystallized matter: from history to applications. *Dalton Trans.* **2016,** *45* (10), 4073-4089.
26. Bousquet, D.; Coudert, F. X.; Fossati, A. G.; Neimark, A. V.; Fuchs, A. H.; Boutin, A., Adsorption induced transitions in soft porous crystals: an osmotic potential approach to multistability and intermediate structures. *J Chem Phys* **2013,** *138* (17), 174706.
27. Coudert, F.-X.; Boutin, A.; Fuchs, A. H.; Neimark, A. V., Adsorption Deformation and Structural Transitions in Metal–Organic Frameworks: From the Unit Cell to the Crystal. *J. Phys. Chem. Lett.* **2013,** *4* (19), 3198-3205.
28. Schneemann, A.; Bon, V.; Schwedler, I.; Senkovska, I.; Kaskel, S.; Fischer, R. A., Flexible metal–organic frameworks. *Chemical Society Reviews* **2014,** *43* (16), 6062-6096.
29. Krause, S.; Bon, V.; Senkovska, I.; Stoeck, U.; Wallacher, D.; Többens, D. M.; Zander, S.; Pillai, R. S.; Maurin, G.; Coudert, F.-X.; Kaskel, S., A pressure-amplifying framework material with negative gas adsorption transitions. *Nature* **2016,** *532*, 348.
30. Férey, G.; Serre, C., Large breathing effects in three-dimensional porous hybrid matter: facts, analyses, rules and consequences. *Chem. Soc. Rev.* **2009,** *38* (5), 1380-1399.
31. Katsoulidis, A. P.; Antypov, D.; Whitehead, G. F. S.; Carrington, E. J.; Adams, D. J.; Berry, N. G.; Darling, G. R.; Dyer, M. S.; Rosseinsky, M. J., Chemical control of structure and guest uptake by a conformationally mobile porous material. *Nature* **2019,** *565* (7738), 213-217.
32. Bueken, B.; Vermoortele, F.; Vanpoucke, D. E.; Reinsch, H.; Tsou, C. C.; Valvekens, P.; De Baerdemaeker, T.; Ameloot, R.; Kirschhock, C. E.; Van Speybroeck, V.; Mayer, J. M.; De Vos, D., A

Flexible Photoactive Titanium Metal-Organic Framework Based on a [Ti(IV)3(mu3-O)(O)2(COO)6] Cluster. *Angew Chem Int Edit* **2015,** *54* (47), 13912-7.

33. Bueken, B.; Vermoortele, F.; Cliffe, M. J.; Wharmby, M. T.; Foucher, D.; Wieme, J.; Vanduyfhuys, L.; Martineau, C.; Stock, N.; Taulelle, F.; Van Speybroeck, V.; Goodwin, A. L.; De Vos, D., A Breathing Zirconium Metal–Organic Framework with Reversible Loss of Crystallinity by Correlated Nanodomain Formation. *Chem-Eur J.* **2016,** *22* (10), 3264-3267.

34. Bai, Y.; Dou, Y.; Xie, L. H.; Rutledge, W.; Li, J. R.; Zhou, H. C., Zr-based metal-organic frameworks: design, synthesis, structure, and applications. *Chem Soc Rev* **2016,** *45* (8), 2327-67.

35. Gu, C.; Hosono, N.; Zheng, J. J.; Sato, Y.; Kusaka, S.; Sakaki, S.; Kitagawa, S., Design and control of gas diffusion process in a nanoporous soft crystal. *Science* **2019,** *363* (6425), 387-391.

36. Furukawa, H.; Gandara, F.; Zhang, Y. B.; Jiang, J.; Queen, W. L.; Hudson, M. R.; Yaghi, O. M., Water adsorption in porous metal-organic frameworks and related materials. *J Am Chem Soc* **2014,** *136* (11), 4369-81.

37. SK, M.; Bhowal, S.; Biswas, S., Synthesis, Characterization, Stability, and Gas Adsorption Characteristics of a Highly Stable Zirconium Mesaconate Framework Material. *Eur. J. Inorg. Chem.* **2015,** *2015* (20), 3317-3322.

38. Wang, S.; Wahiduzzaman, M.; Martineau-Corcos, C.; Maurin, G.; Serre, C., A Microporous Zirconium Metal-Organic Framework Based on Trans-aconitic Acid for Selective Carbon Dioxide Adsorption. *Eur. J. Inorg. Chem.* **2019,** *2019* (22), 2674-2679.

39. Wang, S.; Wahiduzzaman, M.; Davis, L.; Tissot, A.; Shepard, W.; Marrot, J.; Martineau-Corcos, C.; Hamdane, D.; Maurin, G.; Devautour-Vinot, S.; Serre, C., A robust zirconium amino acid metal-organic framework for proton conduction. *Nat Commun* **2018,** *9* (1), 4937.

40. Elsa, A.; Nathalie, G.; Charlotte, M.; Bart, B.; Ben, V. d. V.; Clément, L. G.; Paul, F.; Farid, N.; Francis, T.; Dirk, d. V.; Jong‐San, C.; Ho, C. K.; Naseem, R.; Thomas, D.; Marco, D.; Guillaume, M.; Christian, S., The Structure of the Aluminum Fumarate Metal‐Organic Framework A520. *Angew. Chem. Int. Ed.* **2015,** *54* (12), 3664-3668.

41. Livage, C.; Egger, C.; Nogues, M.; Ferey, G., Hybrid open frameworks (MIL-n). Part 5 - Synthesis and crystal structure of MIL-9: a new three-dimensional ferrimagnetic cobalt(II) carboxylate with a two-dimensional array of edge-sharing Co octahedra with 12-membered rings. *J Mater Chem* **1998,** *8* (12), 2743-2747.

42. Livage, C.; Egger, C.; Férey, G., Hybrid Open Networks (MIL 16): Synthesis, Crystal Structure, and Ferrimagnetism of Co4(OH)2(H2O)2(C4H4O4)3·2H2O, a New Layered Cobalt(II) Carboxylate with 14-Membered Ring Channels. *Chem. Mater.* **1999,** *11* (6), 1546-1550.

43. Wißmann, G.; Schaate, A.; Lilienthal, S.; Bremer, I.; Schneider, A. M.; Behrens, P., Modulated synthesis of Zr-fumarate MOF. *Micropor. Mesopor. Mater.* **2012,** *152*, 64-70.

44. Wang, S.; Kitao, T.; Guillou, N.; Wahiduzzaman, M.; Martineau-Corcos, C.; Nouar, F.; Tissot, A.; Binet, L.; Ramsahye, N.; Devautour-Vinot, S.; Kitagawa, S.; Seki, S.; Tsutsui, Y.; Briois, V.; Steunou, N.; Maurin, G.; Uemura, T.; Serre, C., A phase transformable ultrastable titanium-carboxylate framework for photoconduction. *Nat Commun* **2018,** *9* (1), 1660.

45. Wahiduzzaman, M.; Wang, S.; Sikora, B. J.; Serre, C.; Maurin, G., Computational structure determination of novel metal-organic frameworks. *Chem Commun* **2018,** *54* (77), 10812-10815.

46. Duran, D.; Couster, S. L.; Desjardins, K.; Delmotte, A.; Fox, G.; Meijers, R.; Moreno, T.; Savko, M.; Shepard, W., PROXIMA 2A – A New Fully Tunable Micro-focus Beamline for Macromolecular Crystallography. *J. Phys. Conf. Ser* **2013,** *425* (1), 012005.

47. Cavka, J. H.; Jakobsen, S.; Olsbye, U.; Guillou, N.; Lamberti, C.; Bordiga, S.; Lillerud, K. P., A new zirconium inorganic building brick forming metal organic frameworks with exceptional stability. *J Am Chem Soc* **2008,** *130* (42), 13850-1.
48. Nijem, N.; Wu, H.; Canepa, P.; Marti, A.; Balkus, K. J., Jr.; Thonhauser, T.; Li, J.; Chabal, Y. J., Tuning the gate opening pressure of Metal-Organic Frameworks (MOFs) for the selective separation of hydrocarbons. *J Am Chem Soc* **2012,** *134* (37), 15201-4.
49. Sato, H.; Kosaka, W.; Matsuda, R.; Hori, A.; Hijikata, Y.; Belosludov, R. V.; Sakaki, S.; Takata, M.; Kitagawa, S., Self-accelerating CO sorption in a soft nanoporous crystal. *Science* **2014,** *343* (6167), 167-70.
50. Shimomura, S.; Higuchi, M.; Matsuda, R.; Yoneda, K.; Hijikata, Y.; Kubota, Y.; Mita, Y.; Kim, J.; Takata, M.; Kitagawa, S., Selective sorption of oxygen and nitric oxide by an electron-donating flexible porous coordination polymer. *Nat Chem* **2010,** *2* (8), 633-7.
51. Maji, T. K.; Matsuda, R.; Kitagawa, S., A flexible interpenetrating coordination framework with a bimodal porous functionality. *Nat Mater* **2007,** *6* (2), 142-8.
52. Bae, Y. S.; Farha, O. K.; Spokoyny, A. M.; Mirkin, C. A.; Hupp, J. T.; Snurr, R. Q., Carborane-based metal-organic frameworks as highly selective sorbents for CO(2) over methane. *Chem Commun* **2008,** (35), 4135-7.
53. Heuchel, M.; Snurr, R. Q.; Buss, E., Adsorption of CH4−CF4 Mixtures in Silicalite: Simulation, Experiment, and Theory. *Langmuir* **1997,** *13* (25), 6795-6804.
54. Benoit, V.; Pillai, R. S.; Orsi, A.; Normand, P.; Jobic, H.; Nouar, F.; Billemont, P.; Bloch, E.; Bourrelly, S.; Devic, T.; Wright, P. A.; de Weireld, G.; Serre, C.; Maurin, G.; Llewellyn, P. L., MIL-91(Ti), a small pore metal–organic framework which fulfils several criteria: an upscaled green synthesis, excellent water stability, high CO2 selectivity and fast CO2 transport. *J. Mater. Chem. A* **2016,** *4* (4), 1383-1389.
55. Liu, J.; Thallapally, P. K.; McGrail, B. P.; Brown, D. R.; Liu, J., Progress in adsorption-based CO2 capture by metal-organic frameworks. *Chem Soc Rev* **2012,** *41* (6), 2308-22.